crystals

MDPI

Article

Phase Transition Behavior of the Layered Perovskite $CsBi_{0.6}La_{0.4}Nb_2O_7$: A Hybrid Improper Ferroelectric

Charlotte A. L. Dixon [1], Jason A. McNulty [1], Kevin S. Knight [2,3], Alexandra S. Gibbs [4] and Philip Lightfoot [1,*]

1 School of Chemistry and EaStCHEM, University of St Andrews, St Andrews KY16 9ST, UK; cald@st-andrews.ac.uk (C.A.L.D.); jam242@st-andrews.ac.uk (J.A.M.)
2 Department of Earth Sciences, University College London, Gower Street, London WC1E 6BT, UK; kevinstevenknight@gmail.com
3 Department of Earth Sciences, The Natural History Museum, Cromwell Road, London SW7 5BD, UK
4 ISIS Facility, Rutherford Appleton Laboratory, Chilton, Oxon OX11 0QX, UK; alexandra.gibbs@stfc.ac.uk
* Correspondence: pl@st-andrews.ac.uk; Tel.: +44-1334-463841

Academic Editor: Stevin Snellius Pramana
Received: 20 April 2017; Accepted: 10 May 2017; Published: 13 May 2017

Abstract: The phase behavior of the layered perovskite $CsBi_{0.6}La_{0.4}Nb_2O_7$, of the Dion-Jacobson family, has been studied by high-resolution powder neutron diffraction between the temperatures of 25 < T < 850 °C. At ambient temperature, this material adopts the polar space group $P2_1am$; this represents an example of hybrid improper ferroelectricity caused by the interaction of two distinct octahedral tilt modes. Within the limits of our data resolution, the thermal evolution of the crystal structure is consistent with a first-order transition between 700 and 750 °C, with both tilt modes vanishing simultaneously, leading to the aristotype space group $P4/mmm$. This apparent "avalanche transition" behavior resembles that seen in the related Aurivillius phase $SrBi_2Nb_2O_9$.

Keywords: polar crystal; layered perovskite; hybrid improper ferroelectric; phase transition

1. Introduction

Recent theoretical work has revealed novel mechanisms for designing non-centrosymmetric, polar and potentially ferroelectric materials, based on the coupling of two or more distinct structural distortions ("modes") [1–4]. So-called "hybrid improper ferroelectrics" (HIFs) have now been postulated for several families of layered perovskites, by the coupling of two distinct "octahedral tilt" modes with a polar mode. Although octahedral tilting has been a well-established phenomenon in perovskite crystallography for many years [5–7], in simple three-dimensional ABX_3 perovskites all the simple octahedral tilt schemes (as classified by Howard and Stokes [7]) give rise to strictly centrosymmetric crystals. It is now recognized that in more complex cases, for example cation-ordered or layered perovskites, inversion symmetry may be broken directly by particular combinations of octahedral tilt modes. The concept of HIFs has been typically applied by theorists to mean the imposition of a stable polar ground state in a crystal via the coupling of two or more intrinsically non-polar modes with a polar mode ("tri-linear coupling"), with no requirement for an experimentally-realized polarization reversal. However, such experimental demonstrations of polarization-field hysteresis have now been reported, for example in the Ruddlesden-Popper (RP) phase $Ca_3Ti_2O_7$ [8] and the Dion-Jacobson (DJ) phase $RbBiNb_2O_7$ [9].

Prior to the recent flurry of work from the theoretical standpoint, it was known that ferroelectricity, or at least polarity, co-existed with octahedral tilting in several layered perovskites, the most well-established being the Aurivillius family, exemplified by $SrBi_2Ta_2O_9$ and $Bi_4Ti_3O_{12}$ [10]. Snedden et al. [11] later made the intuitive link between the nature of octahedral tilting in the DJ

phase $CsBiNb_2O_7$ and that in $SrBi_2Ta_2O_9$; both have a tilt system analogous to that described by the Glazer notation $a^-a^-c^+$ in ABX_3 perovskites. This leads to related superlattices and space groups in both $SrBi_2Ta_2O_9$ and $CsBiNb_2O_7$, viz. superlattices of $\sim\sqrt{2}a_t$ x $\sqrt{2}a_t$ x c_t relative to the aristotype tetragonal phase in each case, and polar space groups $A2_1am$ and $P2_1am$ in $SrBi_2Ta_2O_9$ and $CsBiNb_2O_7$, respectively. The nature of these superlattices and the allowed space groups of the possible distorted structures may be systematized by considering which particular distortion modes give rise to the specific tilts within each family of layered perovskites. So, for example, the "out-of-phase tilt", $a^-a^-c^0$, and the "in-phase tilt", $a^0a^0c^+$, correspond to the modes with irreducible representations M_5^- and M_2^+, respectively, for the DJ phases of the type $AA'B_2O_7$, for which the parent phase is described in space group $P4/mmm$ (these are "$n = 2$" examples of the generic DJ composition $AA'_{n-1}B_nO_{3n+1}$, with n representing the number of octahedral layers per perovskite-like block). The coupling of the two modes leads naturally to the polar space group $P2_1am$ for $CsBiNb_2O_7$ and, in principle, permits ferroelectricity. These ideas have been described in more detail by Benedek et al. [3,4].

Although the $a^-a^-c^+$ tilt system is predicted to be a stable option for DJ phases of the type $AA'B_2O_7$, recent experimental work has shown that other related polymorphs are possible, and a tilt system $a^-b^0c^+$, in polar space group $Amm2$, has been reported in $CsLaNb_2O_7$ in the range $350 < T < 550$ K [12] (curiously an earlier single crystal X-ray study of $CsLaNb_2O_7$ reported the adoption of the aristotype tetragonal structure, $P4/mmm$ at 296 K [13]). Moreover, a recent experimental and theoretical study of the triple-layer DJ phase $CsBi_2Ti_2NbO_{10}$ has suggested that a proper rather than improper mechanism drives the polarity of the ambient temperature phase [14]. It is therefore of interest to explore more fully the phase behavior of further examples of the DJ family in order to map out the occurrence of the possible tilt systems, especially those giving rise to polarity, and also the nature of phase transitions in these systems as a function of T.

In our earlier work [11], it was established that both $CsBiNb_2O_7$ and $CsNdNb_2O_7$ adopted the polar $P2_1am$ space group at ambient temperature, with the latter composition displaying a much reduced orthorhombic distortion relative to the former. Later, Fennie and Rabe predicted ferroelectricity in $CsBiNb_2O_7$ from a first-principles DFT study [15]. Our follow-up experimental studies [16] on $CsBiNb_2O_7$ suggested that ferroelectricity was hindered by moisture uptake, leading to proton conductivity and leakage. Nevertheless, a more recent work by Chen et al. [17] did provide experimental evidence for ferroelectricity in this compound. Goff et al. [16], attempted to determine any high temperature phase transitions in $CsBiNb_2O_7$ using powder neutron diffraction: no evidence for phase transitions was identified up to 900 °C, above which sample deterioration precluded further study. By analogy with $CsNdNb_2O_7$, we speculated that La-doping of $CsBiNb_2O_7$ would reduce the orthorhombic distortion such that any phase transition to higher symmetry might be brought down in temperature relative to that of $CsBiNb_2O_7$, and make this transition more amenable to experimental study.

In this paper, we report the phase behavior of $CsBi_{0.6}La_{0.4}Nb_2O_7$; this composition was chosen since $CsBiNb_2O_7$ and $CsLaNb_2O_7$ have been shown to adopt different phases at ambient temperature, and it was anticipated that a phase transition(s) might be observable within a reasonable temperature regime.

2. Results

Ambient temperature structure: Preliminary studies focused on the solid solution $CsBi_{1-x}La_xNb_2O_7$ (see Supplementary Information), which is confirmed to exist for all compositions, $0 < x < 1$. The $x = 0.4$ composition, i.e., $CsBi_{0.6}La_{0.4}Nb_2O_7$, was chosen for further study by high-resolution powder neutron diffraction. Initial analysis of the room-temperature powder neutron diffraction (PND) data assumed the $P2_1am$ model previously identified for $CsBiNb_2O_7$ [11]. Rietveld refinement suggested this model to be correct, with an excellent fit, accounting for all observed peak splittings and superlattice peaks (Figure 1). However, in order for this assignment to be unambiguous, other options need to be considered. There are two aspects to this: first, the unit cell metrics need to be determined and second,

the nature of any characteristic superlattice peaks (especially those arising from octahedral tilting) needs to be established.

Considering the unit cell metrics first: the possible superlattice options to be considered are either an approximate doubling or quadrupling of the unit cell in the *ab* plane; i.e., $a \sim b \sim \sqrt{2}a_t$ or $a \sim b \sim 2a_t$. Superlattices along the *c*-axis are not considered in the simplest scheme (and are not necessary in this case). These two options can easily be distinguished based on related peak splittings observed in the experimental PND data: the $\sqrt{2}a_t$ metric splits peaks of the type (*hhl*) in the parent tetragonal phase, whereas the $2a_t$ metric splits peaks of the type (*h0l*/*0kl*). Specific peaks labelled in Figure 1 confirm unambiguously that an orthorhombic (or lower) symmetry unit cell of metrics $a \sim b \sim \sqrt{2}a_t$, $c \sim c_t$, is required to account for all the observed peak splittings.

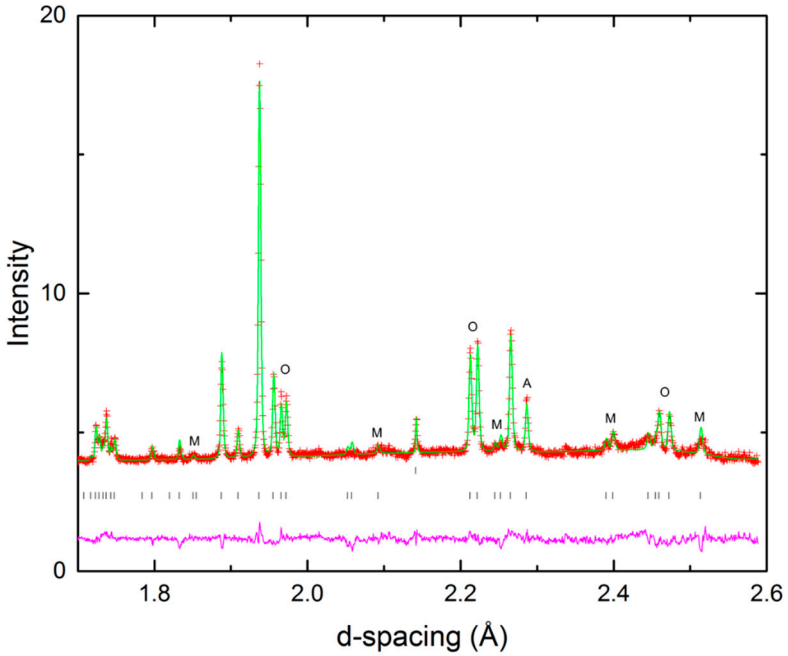

Figure 1. Portion of the Rietveld plot for the $P2_1am$ model at ambient temperature. Peaks marked 'M' represent superlattice peaks at the *M*-point; peaks marked "O" are subcell peaks that split into doublets in this superlattice ($a \sim b \sim \sqrt{2}a_t$), whereas the peak marked "A" represents a peak that would be split if the alternative supercell ($a \sim b \sim 2a_t$) was present. The peak at $d \sim 2.14$ Å is from the vanadium sample holder.

Strayer et al. [12] listed all models corresponding to the simple combinations of octahedral tilts for this structural family (see Supplementary information in Reference [12]). Specifically, the definition of simple combinations here means that there are four distinct octahedral tilts modes to be considered, viz. in-phase and out-of-phase tilts of two adjacent octahedra along the *a* (and/or *b*) and *c* axes of the parent tetragonal unit cell. These four modes are given the Glazer-like symbols a^+ (or b^+) and c^+ for the respective in-phase tilts and a^- (b^-) and c^- for the out-of-phase tilts. In turn, these distortions give rise to superlattice peaks in the diffraction pattern at characteristic points, labelled *M* ($k = \frac{1}{2}, \frac{1}{2}, 0$) or *X* ($k = 0, \frac{1}{2}, 0$) relative to the parent tetragonal reciprocal lattice. The specific modes corresponding to each of the four possible tilts are X_1^+ (a^+), M_5^- (a^-) M_2^+ (c^+) and M_4^- (c^-). The nature of these modes and their effect on the diffraction pattern can be probed using the on-line software ISODISTORT [18]. The *X*-point mode can be easily ruled out (no peaks are visible at the relevant positions), but the *M*-point modes provide some ambiguity, as they may contribute to many of the same superlattice peaks. In fact, closer inspection of the allowed superlattice intensities from each of the *M*-point modes reveals that the M_4^- mode can also be ruled out: we also note that neither the X_1^+ nor the M_4^- modes were considered in the earlier theoretical studies [3,15]. The M_5^- mode is certainly required, as it is

the only contributor to certain peaks (for example the one near d ~2.5 Å). The M_2^+ mode contributes to several observed peaks (for example those near d ~2.4 Å), but the M_5^- mode may also contribute to those. Table 1 lists an abbreviated selection of the possible octahedral-rotation-induced superlattices of Strayer et al. Taking into account the requirement of a $\sqrt{2}a_t$ x $\sqrt{2}a_t$ x c_t orthorhombic metric and the presence of at least the M_5^- mode (and also possibly the M_2^+ mode) reveals the only plausible models are the $P2_1am$ and $Pmam$ ones, as suggested by Snedden et al. [11] for $CsBiNb_2O_7$. In particular, the $Amm2$ model observed for $CsLaNb_2O_7$ can be ruled out in the present case. In order to confirm $P2_1am$ as the correct model for $CsBi_{0.6}La_{0.4}Nb_2O_7$ at ambient temperature, a comparative refinement against the $Pmam$ model was carried out. This led to agreement factors of χ^2 ~5.870 and 9.081, for the $P2_1am$ and $Pmam$ models. $P2_1am$ is therefore selected as the best model at ambient T. The corresponding crystal structure is shown in Figure 2, refined atomic parameters are given in Table 2 and selected bond lengths in Table 3.

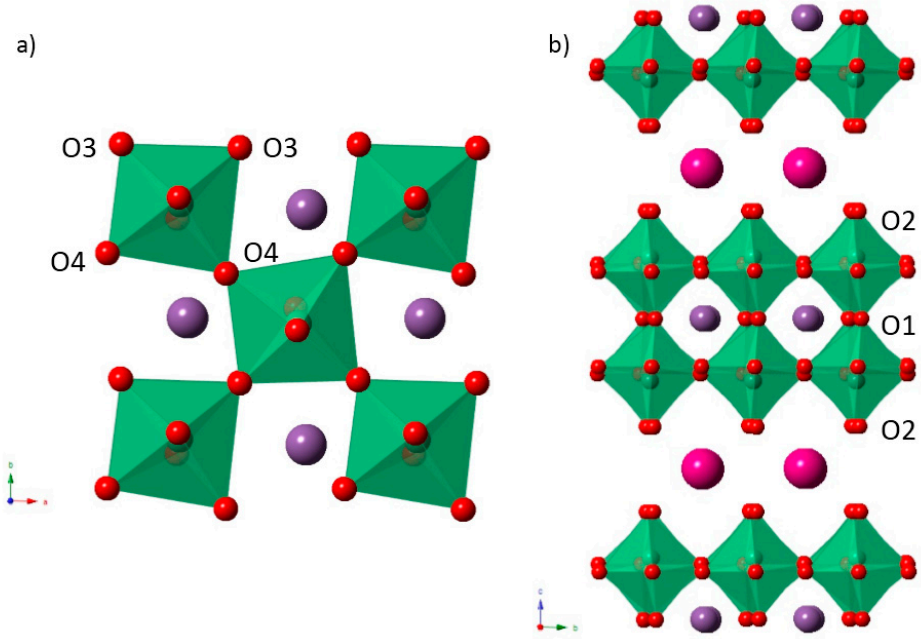

Figure 2. Crystal structure of $CsBi_{0.6}La_{0.4}Nb_2O_7$ at ambient temperature (**a**) down the c-axis, showing the in-phase (M_2^+) tilt and (**b**) perpendicular view, showing the out-of-phase (M_5^-) tilt.

Table 1. Example models based on combinations of octahedral tilt modes (adapted from Strayer et al. [12].)

Glazer Notation	Active Modes	Space Group	Metrics
$a^0a^0c^0$	None	$P4/mmm$	a_t x a_t x c_t
$a^0a^0c^+$	M_2^+	$P4/mbm$	$\sqrt{2}a_t$ x $\sqrt{2}a_t$ x c_t
$a^0a^0c^-$	M_4^-	$P4/nbm$	$\sqrt{2}a_t$ x $\sqrt{2}a_t$ x c_t
$a^+a^+c^0$	X_1^+	$P4/mmm$	$2a_t$ x $2a_t$ x c_t
$a^-a^-c^0$	M_5^-	$Pmam$	$\sqrt{2}a_t$ x $\sqrt{2}a_t$ x c_t
$a^-a^-c^+$	$M_2^+ \otimes M_5^-$	$P2_1am$	$\sqrt{2}a_t$ x $\sqrt{2}a_t$ x c_t
$a^-b^0c^0$	M_5^-	$Cmmm$	$2a_t$ x $2a_t$ x c_t
$a^-b^0c^+$	$M_2^+ \otimes M_5^-$	$Amm2$ *	c_t x $2a_t$ x $2a_t$
$a^-b^-c^0$	M_5^-	$P2/m$	$\sqrt{2}a_t$ x c_t x $\sqrt{2}a_t$
$a^-b^-c^+$	$M_2^+ \otimes M_5^-$	Pm	$\sqrt{2}a_t$ x c_t x $\sqrt{2}a_t$

* $C2mm$ setting for c corresponding to c_t.

Table 2. Refined structural model for $CsBi_{0.6}La_{0.4}Nb_2O_7$ at 25 °C. Space group $P2_1am$, a = 5.49618 (14), b = 5.46012 (14), c = 11.3254 (3) Å.

Atom	Wyckoff Position	x	y	z	100 * U_{iso} (Å^2)
Cs1	2b	0.3349 (17)	0.2579 (12)	0.5	2.08 (10)
Bi/La1 *	2a	0.367	0.2692 (8)	0.0	2.91 (11)
Nb1	4c	0.3334 (10)	0.7540 (6)	0.20533 (14)	0.56 (7)
O1	2a	0.321 (2)	0.6892 (9)	0.0	2.83 (15)
O2	4c	0.3272 (12)	0.7812 (7)	0.3574 (2)	1.66 (9)
O3	4c	0.0869 (15)	0.0104 (12)	0.1589 (3)	3.10 (13)
O4	4c	0.5290 (11)	0.4590 (8)	0.1840 (3)	2.25 (13)

* fixed occupancy $Bi_{0.6}La_{0.4}$; the x-coordinate is fixed to define the origin of the polar axis.

Table 3. Selected bond lengths (Å) for $CsBi_{0.6}La_{0.4}Nb_2O_7$ at 25 °C in the $P2_1am$ model.

Cs-O	Bond Length (Å)	Bi/La-O	Bond Length (Å)	Nb-O	Bond Length (Å)
Cs1-O2 × 2	3.063 (7)	Bi1-O1	2.307 (7)	Nb1-O1	2.3531 (19)
Cs1-O2 × 2	3.158 (10)	Bi1-O1	2.508 (12)	Nb1-O2	1.730 (3)
Cs1-O2 × 2	3.231 (10)	Bi1-O3 × 2	2.651 (6)	Nb1-O3	1.968 (9)
Cs1-O2 × 2	3.282 (7)	Bi1-O3 × 2	2.758 (6)	Nb1-O3	2.018 (8)
		Bi1-O4 × 2	2.492 (4)	Nb1-O4	1.952 (6)
				Nb1-O4	2.052 (6)

Structural Evolution Versus T: The continued presence of orthorhombic distortion can easily be determined on raising the temperature, by tracking the O peak splittings highlighted in Figure 1. However, since the M-point superlattice peaks are very weak, even at ambient temperature, it is problematic to use a simple qualitative visual observation of these as a single reliable measure of the structural distortions versus T. Instead, full comparative Rietveld refinement of the structure in both $P2_1am$ and $Pmam$ models is the preferred method of discrimination (since the tilts significantly affect the intensities of the subcell peaks, in addition to the supercell peaks). Both models were therefore refined against each data set up to 725 °C, taking care to use a consistent set of parameters throughout (see Experimental). At 700 °C the orthorhombic splitting is still clearly seen in the raw data, but at 725 °C the splitting disappears, and the unit cell becomes metrically tetragonal (Figure 3). The parent $P4/mmm$ model was therefore trialed at 725 °C and above, with a further check on the alternative possible tetragonal model, $P4/mbm$ ($a^0a^0c^+$, Table 1) at 725 °C only. In addition to tracking the comparative fit quality for the two orthorhombic models, ISODISTORT was used to derive the mode amplitudes versus T. Thermal evolution of the unit cell parameters is given in Figure 4, and for the distortion modes in Figure 5. Comparative goodness-of-fit parameters (χ^2) for the $P2_1am$ and $Pmam$ models are given in Figure 6.

The difference in χ^2 values clearly supports the assignment of the $P2_1am$ rather than the $Pmam$ model up to 700 °C (χ^2 values are 2.055 and 2.273 for $P2_1am$ and $Pmam$, respectively, at 700 °C). In addition, the tilt mode amplitudes (Figure 5) tend towards zero, but do not become zero, at 700 °C. The negligible difference in fit quality between the four models tested at 725 °C (χ^2 values 2.065, 2.054, 2.041 and 1.883 for $P4/mmm$, $P4/mbm$, $Pmam$ and $P2_1am$, respectively) supports the absence of both tilt modes at this temperature (we note that the refinement in the $P2_1am$ model was unstable to the refinement of thermal parameters, thus a direct comparison is not possible). Although the unit cell volume has no clear discontinuity within the temperature resolution of our datasets, the fact that the polar mode Γ_5^- seems to have a step-like change at the transition may indicate the existence of a first-order component.

We attempted to fit the thermal evolution of the tilt modes, M_2^+ and M_5^-, to critical behavior of the form: amplitude = A $(T_c - T)^\beta$. This produced the fit parameters of A = 0.0292, 0.227; T_C = 749, 742 °C; β = 0.401, 0.127 for the M_2^+ and M_5^- modes, respectively. The key observation here is that the derived value of T_C is approximately equal for the two modes, implying that they condense simultaneously. Unfortunately, the paucity of data in the vicinity of T_C prohibits a definitive conclusion about the exact

T_C and β values, and also the specific mode which drives the transition. However, further support for our crystallographic model comes from a measurement of dielectric properties versus *T*. Figure 7 shows a single dielectric maximum just below 750 °C, with no evidence of any lower temperature anomalies. This supports an abrupt, single phase transition, as was observed crystallographically.

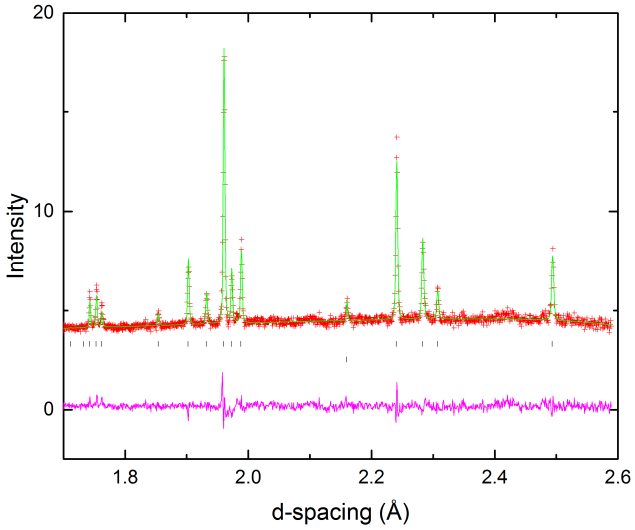

Figure 3. Portion of the Rietveld plot for the *P*4/*mmm* model at 725 °C. Note the absence of both M superlattice peaks and O splittings, compared to Figure 1.

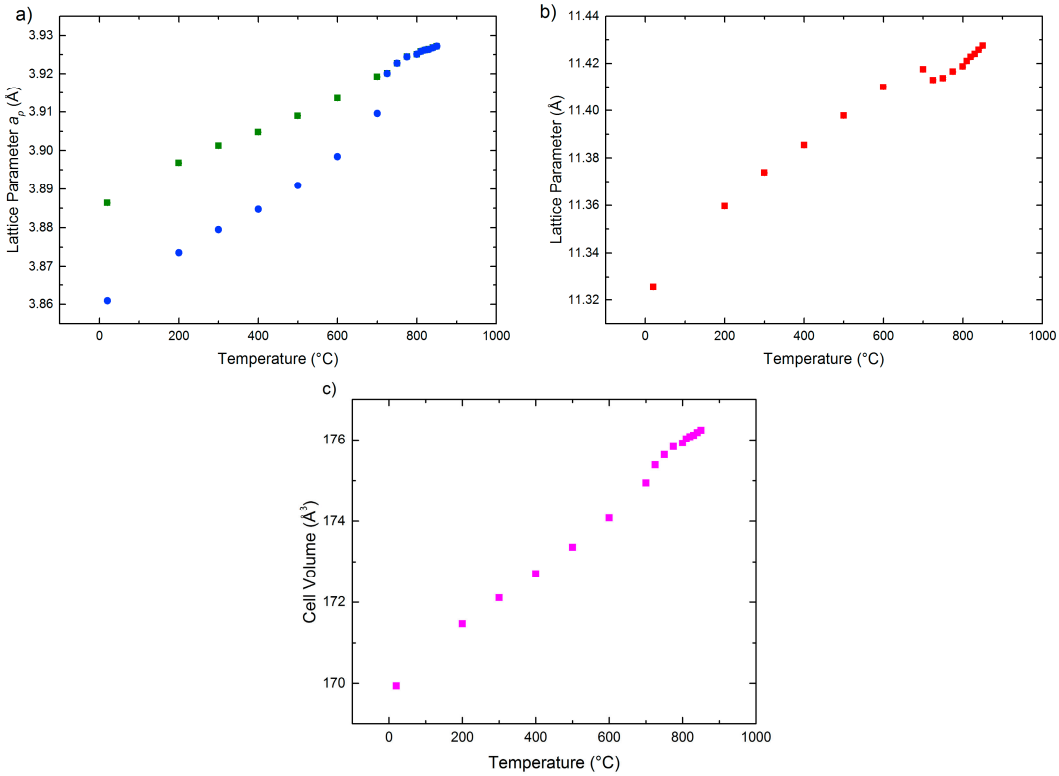

Figure 4. Thermal evolution of the unit cell parameters. (**a**) *a* (squares) and *b* (circles) parameters; (**b**) *c* parameter; (**c**) unit cell volume, suggesting a first-order orthorhombic-tetragonal phase transition near 725 °C. Note that the *a* and *b* parameters in the orthorhombic phase are normalized to the tetragonal subcell (i.e., divided by $\sqrt{2}$).

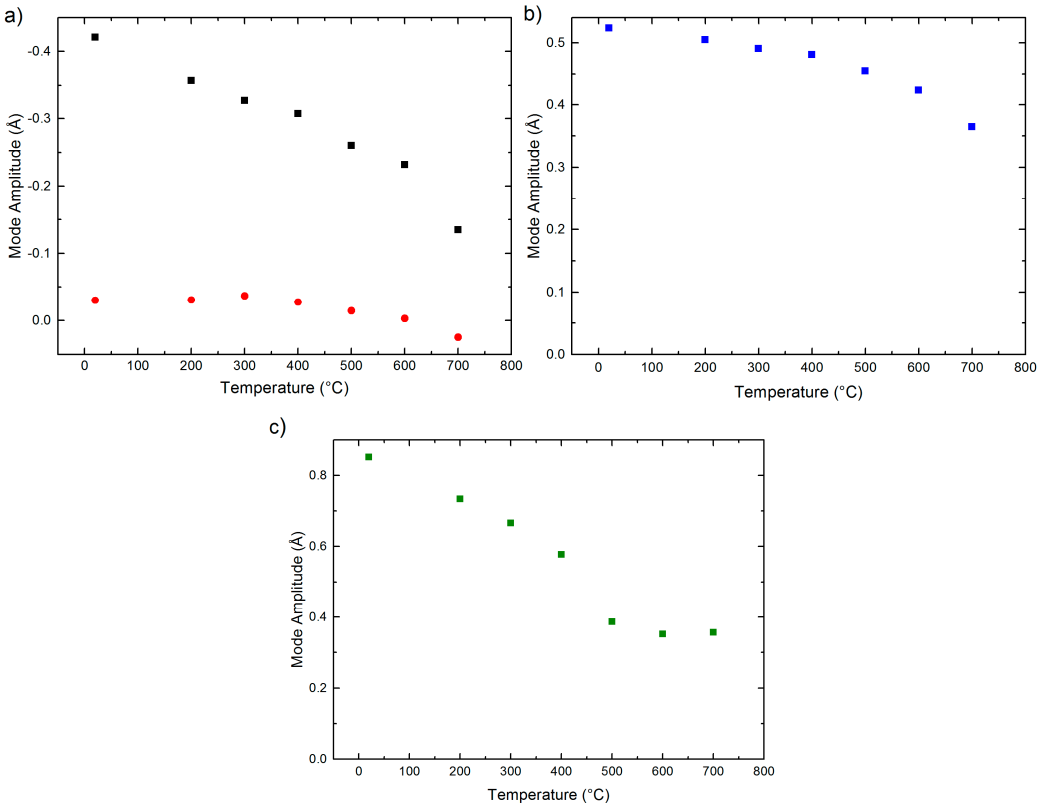

Figure 5. Thermal evolution of the mode amplitudes (from ISODISTORT). (**a**) M_2^+ (squares) and M_3^+ (circles) modes: M_2^+ is the in-phase tilt around *c*, M_3^+ is a minor octahedral distortion mode; (**b**) M_5^- mode: this mode is largely composed of contributions from the out-of-phase tilt around the *ab* plane, but also incorporates minor contributions from antiferrodistortive cation displacements along *b*; (**c**) Γ_5^- mode: this is the polar mode (i.e., polar displacive contributions from all atoms along the *a*-axis).

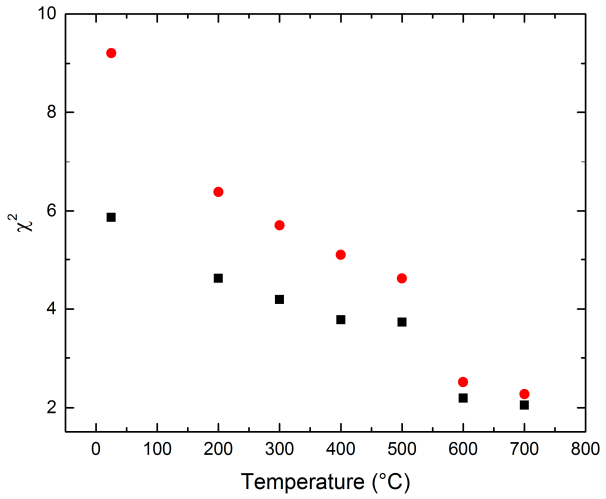

Figure 6. Comparison of Rietveld goodness-of-fit parameters (χ^2) for the $P2_1am$ and *Pmam* models up to a temperature of 700 °C.

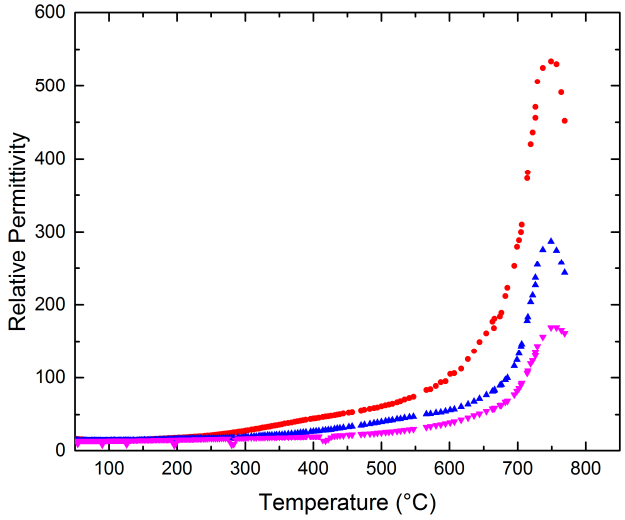

Figure 7. Relative permittivity data for $CsBi_{0.6}La_{0.4}Nb_2O_7$ at selected frequencies, obtained on cooling. Data collected at a frequency of 10 kHz are shown by red circles, 100 kHz by blue triangles and 1 MHz by pink triangles.

Taken together, these observations suggest a direct to transition from $P2_1am$ to $P4/mmm$ in the vicinity of 700–750 °C; we note that Landau theory requires the direct $P2_1am$ to $P4/mmm$ transition to be first-order, whereas the $Pmam$ to $P4/mmm$ transition is allowed to be continuous. Hence, the most likely scenario, which is also compatible with the present data, is that both tilt modes are lost simultaneously, with no substantial evidence for an intermediate phase of symmetry $Pmam$ or $P4/mbm$ (Table 1). The final refined model in $P4/mmm$ at 750 °C is given in Tables 4 and 5.

Table 4. Refined structural model for $CsBi_{0.6}La_{0.4}Nb_2O_7$ at 750 °C. Space group $P4/mmm$, a = 3.92282 (16), c = 11.4138 (5) Å.

Atom	Wyckoff Position	x	y	z	100 * U_{iso} (Å^2)
Cs1	1b	0.0	0.0	0.5	7.09 (13)
Bi/La1 *	1a	0.0	0.0	0.0	7.17 (16)
Nb1	2h	0.5	0.5	0.20414 (16)	2.13 (9)
O1	4i	0.0	0.5	0.17054 (17)	5.56 (10)
O2	2h	0.5	0.5	0.3555 (3)	6.44 (13)
O3	1c	0.5	0.5	0.0	7.20 (17)

* fixed occupancy $Bi_{0.6}La_{0.4}$.

Table 5. Selected bond lengths (Å) for $CsBi_{0.6}La_{0.4}Nb_2O_7$ at 750 °C in the $P4/mmm$ model.

Cs-O	Bond Length (Å)	Bi/La-O	Bond Length (Å)	Nb-O	Bond Length (Å)
Cs1-O2 × 8	3.2273 (14)	Bi1-O1 × 8	2.7634 (14)	Nb1-O1 × 4	1.9985 (5)
		Bi1-O3 × 4	2.77385 (11)	Nb1-O2	1.727 (4)
				Nb1-O3	2.3300 (18)

3. Discussion and Conclusions

The present study indicates, within the temperature resolution of our data, a direct first-order transition from the parent, untilted phase, $P4/mmm$, to the observed ambient temperature phase, $P2_1am$ (tilt system $a^-a^-c^+$). This requires the simultaneous condensation of the two tilt modes M_5^- ($a^-a^-c^0$) and M_2^+ ($a^0a^0c^+$), which couple with the polar mode, Γ_5^-. This special case of tri-linear coupling has been termed an "avalanche transition" [19]. Due to the temperature increments used in

this experiment, we cannot fully rule out a possible intermediate phase of symmetry *Pmam* or *P*4/*mbm* but, if present, this must only exist in a narrow temperature interval around 700 to 750 °C. Avalanche transitions are rare, but such a transition has been confirmed in the Aurivillius phase ferroelectric, $SrBi_2Nb_2O_9$ [20,21], which also displays the tilt system $a^-a^-c^+$. It has been suggested that $SrBi_2Nb_2O_9$ differs from its analogue $SrBi_2Ta_2O_9$, which does display an intermediate phase (tilt system $a^-a^-c^0$), because the magnitudes of the three necessary distortion modes in the ground state (i.e., ambient temperature) polar phase are relatively similar, rather than one tilt mode being dominant [21]. In their detailed study of $CsLaNb_2O_7$, Strayer et al. [12], reported a tilt system $a^-b^0c^+$ (space group *Amm*2, Table 1) between 550 and 350 K. This phase also requires the condensation of both the M_2^+ and M_5^- tilt modes, but differs from the present $P2_1am$ phase in the direction of the M_5^- mode. It might also be expected that an intermediate phase would be observed in the *P*4/*mmm* to *Amm*2 pathway seen in $CsLaNb_2O_7$; i.e., via the sequential loss of either M_5^- then M_2^+, or vice versa. The corresponding intermediate phases (Table 1) in that case would be $a^0a^0c^+$ (*P*4/*mbm*) or $a^-b^0c^0$ (*Cmmm*). Strayer et al. ruled out these pathways by the observation of a clear SHG signal, signifying non-centrosymmetricity, and thus implying an avalanche transition in this composition also. As the present study represents the only detailed crystallographic study so far of the tilt transitions concerning a verified $P2_1am$ phase ($a^-a^-c^+$) in the n = 2 DJ family, it remains to be seen whether such avalanche transitions are common in the DJ family.

4. Experimental Section

4.1. Synthesis

A phase pure sample of $CsBi_{0.6}La_{0.4}Nb_2O_7$ was prepared using traditional ceramic methods. Stoichiometric amounts of La_2O_3 (99.9% Sigma-Aldrich, Dorset, UK, Nb_2O_5 (99.9% Alfa Aesar, Lancashire, UK) and a 20% excess of Cs_2CO_3 (99% Alfa Aesar, Lancashire, UK) were dried at 100 °C for 24 h. The loose powders were ground for a period of 30 min and pressed into pellets of approximately 10 mm diameter and 5 mm thickness. The pellets were annealed at 1000 °C for a period of 24 h with a cooling rate of 10 min^{-1}.

4.2. Powder Diffraction

Sample purity was gauged by preliminary X-ray diffraction using a PANalytical Empyrean (Cu $K_{\alpha 1}$ radiation).

Neutron powder diffraction (NPD) was performed at beamline HRPD (High resolution powder diffractometer), ISIS facility, Oxfordshire, UK. A sample of approximately 5 g was placed in an 8-mm cylindrical vanadium can before loading into the diffractometer vacuum furnace. Patterns were collected at room temperature, and then at 100 intervals between 200–800 °C with a final data collection at 850 °C, each data collection lasting approximately 3.5 h, with the exception of the data collections at 600 and 700 °C (which lasted approximately 2 h). Intermediate patterns were collected at intervals of 10 between 810 and 840 °C, and 25 intervals between 725 and 775 °C, each data collection lasting approximately 25 min.

Rietveld refinement was performed using GSAS [22] and the EXPGUI interface [23]. The same set of standard parameters were used, including 3, 3, 21 and 5 parameters to model instrumental variables, scale factors, background and peak-shape for each dataset in the region of RT to 700 °C. The same refinement strategy was employed for the remaining high temperature datasets, except that the number of background terms was decreased from 21 to 18. A significant contribution from the vanadium sample can was seen throughout and this was fitted as a secondary phase at each temperature.

4.3. Dielectric Measurements

Pellets were electroded with sputtered Au before being coated with Ag paste (RS components). Dielectric measurements were made using a Wayne Kerr 6500B impedance analyzer with the sample

mounted in a tube furnace. Capacitance and loss data were recorded in the frequency range of 100–10 MHz at a heating and cooling at a rate of 2 K min^{-1} over the temperature range of 50 to approximately 750 °C. Data collected on the cooling cycle are described here, since the heating cycle showed an additional anomaly due to the failure of the Ag paste (which is used to protect the Au electrode). Nevertheless, there was no evidence for hysteresis during the heating/cooling cycle.

Supplementary Materials: The following are available online at http://www.mdpi.com/2073-4352/7/5/135/s1, Figure S1: (**a**) normalised *a* (black squares) and *b* (red circles) lattice parameters obtained for varying values of *x* across the solid solution $CsBi_{1-x}La_xNb_2O_7$, (**b**) *c* lattice parameter for varying values of *x* and (**c**) (normalized) unit cell volume for varying values of *x*.

Acknowledgments: We thank EPSRC for a Ph.D. studentship to CALD (EP/P505097/1). We thank undergraduate students William Skinner and Adam Smyth for some preliminary work on the $CsBi_{1-x}La_xNb_2O_7$ solid solution and Finlay D. Morrison for guidance on the dielectric measurements.

Author Contributions: Charlotte A. L. Dixon carried out the synthesis and diffraction measurements. Kevin S. Knight and Alexandra S. Gibbs assisted with collection of neutron diffraction data and Jason A. McNulty carried out the dielectric measurements. Charlotte A. L. Dixon carried out the crystallographic analysis, with the assistance of Philip Lightfoot. Philip Lightfoot coordinated the project and wrote the paper, with the approval of all authors.

Conflicts of Interest: The authors declare no conflict of interest.

Appendix A

Further details of the crystal structures at selected temperatures may be obtained from Fachinformationszentrum (FIZ) Karlsruhe, 76344 Eggenstein-Leopoldshafen, Germany (e-mail: crysdata@fiz-karlsruhe.de) on quoting deposition numbers 432943-432945. The research data (raw neutron diffraction data) pertaining to this paper are available at http://dx.doi.org/10.17630/404e3a8f-3346-4dcc-b90a-62795097b1eb.

References

1. Benedek, N.A.; Fennie, C.J. Hybrid improper ferroelectricity: A mechanism for controllable polarization-magnetization coupling. *Phys. Rev. Lett.* **2011**, *106*, 107204. [CrossRef] [PubMed]
2. Bousquet, E.; Dawber, M.; Stucki, N.; Lichtensteiger, C.; Hermet, P.; Gariglio, S.; Triscone, J.-M.; Ghosez, P. Improper ferroelectricity in perovskite oxide artificial superlattices. *Nature* **2008**, *452*, 732–736. [CrossRef] [PubMed]
3. Benedek, N.A. Origin of Ferroelectricity in a Family of Polar Oxides: The Dion—Jacobson Phases. *Inorg. Chem.* **2014**, *53*, 3769–3777. [CrossRef] [PubMed]
4. Benedek, N.A.; Rondinelli, J.M.; Djani, H.; Ghosez, P.; Lightfoot, P. Understanding ferroelectricity in layered perovskites: New ideas and insights from theory and experiments. *Dalton Trans.* **2015**, *44*, 10543–10558. [CrossRef] [PubMed]
5. Glazer, A.M. The classification of tilted octahedra in perovskites. *Acta Crystallogr.* **1972**, *B28*, 3384–3392. [CrossRef]
6. Woodward, P.M. Octahedral Tilting in Perovskites. I. Geometrical Considerations. *Acta Crystallogr.* **1997**, *B53*, 32–43. [CrossRef]
7. Howard, C.J.; Stokes, H.T. Group-theoretical analysis of octahedral tilting in perovskites. *Acta Crystallogr.* **1998**, *B54*, 782–789. [CrossRef]
8. Oh, Y.S.; Luo, X.; Huang, F.-T.; Wang, Y.; Cheong, S.-W. Experimental demonstration of hybrid improper ferroelectricity and the presence of abundant charged walls in (Ca, Sr) $_3Ti_2O_7$ crystals. *Nat. Mater.* **2015**, *14*, 407–413. [CrossRef] [PubMed]
9. Li, B.-W.; Osada, M.; Ozawa, T.C.; Sasaki, T. $RbBiNb_2O_7$: A New Lead-Free High-T c Ferroelectric. *Chem. Mater.* **2012**, *24*, 3111–3113. [CrossRef]
10. Withers, R.L.; Thompson, J.G.; Rae, A.D. The crystal chemistry underlying ferroelectricity in $Bi_4Ti_3O_{12}$, Bi_3TiNbO_9, and Bi_2WO_6. *J. Solid State Chem.* **1991**, *94*, 404–417. [CrossRef]
11. Snedden, A.; Knight, K.S.; Lightfoot, P. Structural distortions in the layered perovskites $CsANb_2O_7$ (A= Nd, Bi). *J. Solid State Chem.* **2003**, *173*, 309–313. [CrossRef]

12. Strayer, M.E.; Gupta, A.S.; Akamatsu, H.; Lei, S.; Benedek, N.A.; Gopalan, V.; Mallouk, T.E. Emergent Noncentrosymmetry and Piezoelectricity Driven by Oxygen Octahedral Rotations in n = 2 Dion–Jacobson Phase Layer Perovskites. *Adv. Funct. Mater.* **2016**, *26*, 1930. [CrossRef]
13. Kumada, N.; Kinomura, N.; Sleight, A.W. $CsLaNb_2O_7$. *Acta Crystallogr.* **1996**, *C52*, 1063–1065. [CrossRef]
14. McCabe, E.E.; Bousquet, E.; Stockdale, C.P.J.; Deacon, C.A.; Tran, T.T.; Halasyamani, P.S.; Stennett, M.C.; Hyatt, N.C. Proper Ferroelectricity in the Dion–Jacobson Material $CsBi_2Ti_2NbO_{10}$: Experiment and Theory. *Chem. Mater.* **2015**, *27*, 8298–8309. [CrossRef]
15. Fennie, C.J.; Rabe, K.M. Ferroelectricity in the Dion-Jacobson $CsBiNb_2O_7$ from first principles. *Appl. Phys. Lett.* **2006**, *88*, 262902. [CrossRef]
16. Goff, R.J.; Keeble, D.; Thomas, P.A.; Ritter, T.; Morrison, F.D.; Lightfoot, P. Leakage and proton conductivity in the predicted ferroelectric $CsBiNb_2O_7$. *Chem. Mater.* **2009**, *21*, 1296–1302. [CrossRef]
17. Chen, C.; Ning, H.; Lepadatu, S.; Cain, M.; Yan, H.; Reece, M.J. Ferroelectricity in Dion–Jacobson $ABiNb_2O_7$ (A= Rb, Cs) compounds. *J. Mater. Chem.* **2015**, *3*, 19–22. [CrossRef]
18. Campbell, B.J.; Stokes, H.T.; Tanner, D.E.; Hatch, D.M. ISODISPLACE: A web-based tool for exploring structural distortions. *J. Appl. Crystallogr.* **2006**, *39*, 607. [CrossRef]
19. Etxebarria, I.; Perez-Mato, J.M.; Boullay, P. The role of trilinear couplings in the phase transitions of Aurivillius compounds. *Ferroelectrics* **2010**, *401*, 17–23. [CrossRef]
20. Snedden, A.; Hervoches, C.H.; Lightfoot, P. Ferroelectric phase transitions in $SrBi_2Nb_2O_9$ and $Bi_5Ti_3FeO_{15}$: A powder neutron diffraction study. *Phys. Rev. B* **2003**, *67*, 092102. [CrossRef]
21. Boullay, P.; Tellier, J.; Mercurio, D.; Manier, M.; Zuñiga, F.J.; Perez-Mato, J.M. Phase transition sequence in ferroelectric Aurivillius compounds investigated by single crystal X-ray diffraction. *Solid State Sci.* **2012**, *14*, 1367–1371. [CrossRef]
22. Larson, A.C.; von Dreele, R.B. *General Structure Analysis System (GSAS)*; Los Alamos National Laboratory Report No. 88-748; Los Alamos National Laboratory: Los Alamos, NM, USA, 1994.
23. Toby, B.H. EXPGUI, a graphical user interface for GSAS. *J. Appl. Crystallogr.* **2001**, *34*, 210–213. [CrossRef]